Monte Carlo study of effective mobility in short channel FDSOI MOSFETs

Sébastien Guarnay*‡, François Triozon*, Sébastien Martinie*, Yann-Michel Niquet†, and Arnaud Bournel‡

*CEA, LETI, MINATEC Campus, 17 rue des Martyrs, 38054 Grenoble, France
† CEA, UJF, INAC, SP2M/L_Sim, 17 rue des Martyrs, 38054 Grenoble, France
‡ Institut d'Électronique Fondamentale, Université Paris-Sud, UMR CNRS 8622, Bât. 220, 91405 Orsay, France
Email: sebastien.guarnay@cea.fr

***Abstract*—Quasi-ballistic electron transport in ultrashort FDSOI devices is analyzed using Multi-Subband Monte Carlo (MSMC) simulations, taking into account the main scattering mechanisms: phonons, surface roughness, and charged impurities in the access regions. In particular, the ballistic resistance (defined as the resistance of the channel in absence of scattering) was extracted from ballistic simulations, and shown to be in good agreement with an accurate analytical model including the contact resistance effect. The simulations show an apparent mobility degradation when the channel length decreases, comparable to that observed in experiments, without requiring any additional scattering mechanism in order to explain it.**

Keywords—MOSFET; FDSOI; mobility degradation; analytical model; contact resistance; ballistic; multi-subband Monte Carlo; simulation.

I. Introduction

The reduction of the MOSFET channel length leads to a degradation of the apparent carrier mobility extracted from electrical measurements [1, 2]. Several possible contributions to this mobility decrease have been investigated theoretically. Some of them are related to the mobility extraction method itself, which may underestimate the effect of "ballistic" [3, 4] and contact [5] resistances, both becoming important in short channel devices. Other contributions could arise from additional scattering centers induced by the technological process, such as neutral defects [2, 6].

In the present study, we have evaluated accurately the relative contributions of contact and ballistic resistances, and carrier scattering in N-type FDSOI devices with different channel lengths. For this purpose, Multi-Subband Monte Carlo (MSMC) simulations have been performed, taking into account the main scattering mechanisms, such as charged impurities in the access regions, and Pauli exclusion principle [7]. Furthermore, the ballistic resistance (defined as the resistance of the channel in absence of scattering) was extracted from ballistic simulations, and compared to an accurate analytical model.

II. Multi-Subband Monte Carlo Simulations

The MSMC method takes into account quantum confinement while treating carrier transport semi-classically. It was applied to the N-type FDSOI transistors of Fig. 1 with channel lengths L going from 10 to 200 nm. Source and drain are doped at 10^{20} cm^{-3} and the channel is undoped. All simulations were performed at back-gate bias $V_{bg} = 0$ V and source-drain bias $V_{ds} = 50$ mV. The effective mass approximation was used to describe the six "Δ" valleys of electrons in silicon. The 1D Schrödinger equation is solved along the confinement direction, at each position x along the channel, in order to provide the subbands' energies and the spatial repartition of the wavefunctions. Phonon, surface roughness, and ionized impurity scattering were included, using the models of Ref. [8]. Device simulations were performed with or without scattering in the channel, as illustrated in Figs. 2 and 3. Scattering was always included in the access regions, in order to stabilize convergence of the electrostatic potential. The random choice of scattering events satisfies the Pauli exclusion principle, allowing only transitions towards unoccupied states, although this did not make a qualitative difference on the simulation results.

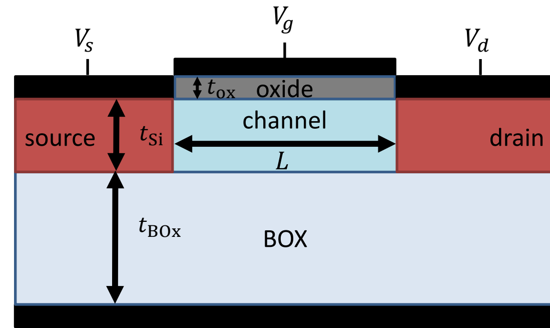

Figure 1. Fully Depleted MOSFET and definition of the main geometrical parameters. $t_{Si} = 4$ nm, $t_{BOX} = 10$ nm and $t_{ox} = 1$ nm. The substrate has orientation (001) and transport direction ⟨100⟩. The source and drain are heavily doped with abrupt concentration profile.

Simulations under frozen vertical field and uniform longitudinal driving field were also performed in order to evaluate accurately the long channel mobility. This method mimics an infinite, junctionless, channel. The vertical field is calculated self-consistently with the Schrödinger equation, as in device simulations.

978-1-4799-5288-5/14/$31.00 © 2014 IEEE

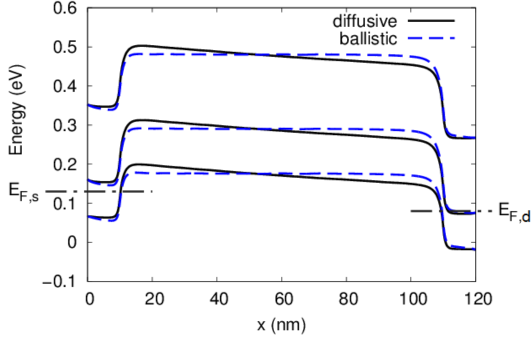

Figure 2. Energy of the three lowest subbands of the Δ_z valleys (z is the confinement direction). $L = 100$ nm. $V_g = 0.2$ V. $V_{ds} = 50$ mV. The energy levels in ballistic device simulations are flat because no scattering allows for an equilibrium.

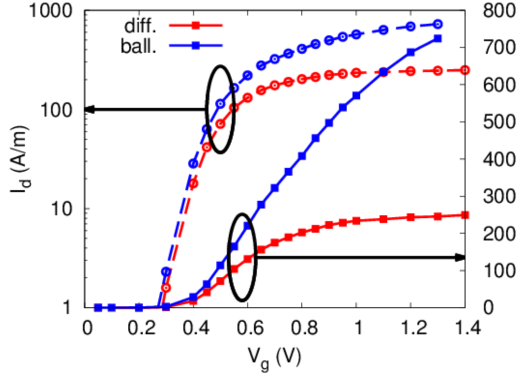

Figure 3. Comparison of diffusive and ballistic currents. Right: linear scale. Left: log. scale. $L = 30$ nm.

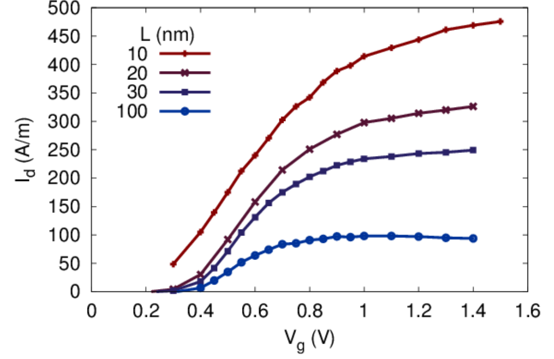

Figure 4. $I_d(V_g)$ at different channel lengths (nm) with scattering in the channel. $L = 10, 20, 30$ and 100 nm. $V_{ds} = 50$ mV.

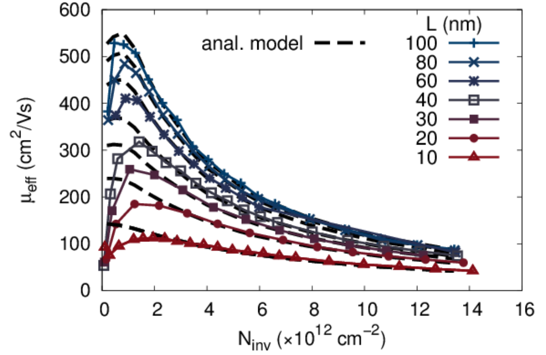

Figure 5. Effective mobility extracted from simulations with scattering in the channel. Solid line: Monte Carlo simulation. Dotted line: analytical model (Eqs. 2 and 3).

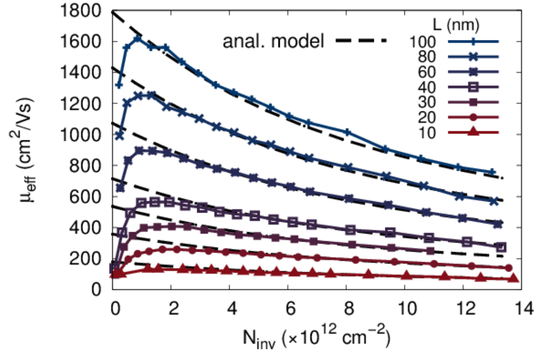

Figure 6. Effective mobility extracted from simulations with ballistic channel. Solid line: Monte Carlo simulation. Dotted lines: analytical model (Eqs. 1 and 3).

III. Results and Discussion

We first present the MSMC device simulations with all scattering mechanisms activated. Fig. 4 shows the $I_d(V_g)$ characteristics for different gate lengths. The effective mobility μ_{eff}, shown in Fig. 5, was extracted from the current and the inversion charge N_{inv}, in analogy to split CV measurements [9]. This method allows for an accurate mobility extraction compared to the Hamer [10] and Y function [11] methods, because there is no assumption on the current model, especially on the charge, to extract the mobility. The length dependence of the effective mobility is shown in Fig. 7 at different inversion charge N_{inv}. It is comparable to experiments highlighting the mobility degradation in short channel devices [2]. As expected, the mobility decreases with N_{inv}, because of the phonon and surface roughness scattering. The mobility degradation varies with the inversion charge and the global decrease (normalized $\Delta\mu$) between long and short channel mobility is slightly reduced for higher N_{inv}.

Conversely to split CV measurements, there should not be parasitic effects in the charge evaluation which lead to a non-physical vanishing of the mobility at low inversion. Indeed, the charge was evaluated in a central region of the channel where the surface charge density is nearly constant, excluding the proximity (in our case 2nm) of the junctions with doped access regions. However, the charge remains overestimated due to the noise inherent to MSMC simulations, which might explain in part why the mobility decreases anyway. Finally, in classical methodology, it seems clear that the degradation is under- or overestimated due to a wrong inversion charge evaluation.

According to Shur's approach [3], the $\mu(L)$ variations (as in Fig. 7) are then analyzed by a Matthiessen-like fit $\frac{1}{\mu(N_{inv},L)} = \frac{1}{K_{bal}L} + \frac{1}{\mu_{\text{long}}(N_{inv})}$ where $K_{bal}L$ and μ_{long} are the ballistic and diffusive components of the mobility,

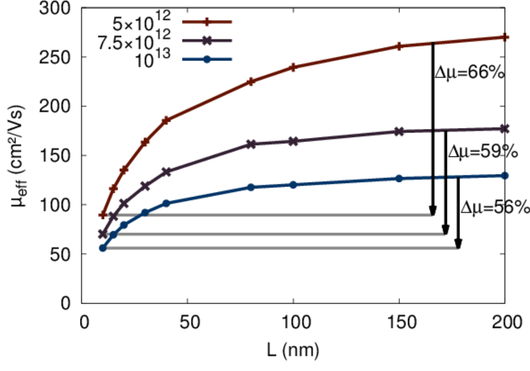

Figure 7. Mobility vs. gate length at different N_{inv} (cm^{-2}), extracted from Monte Carlo simulation.

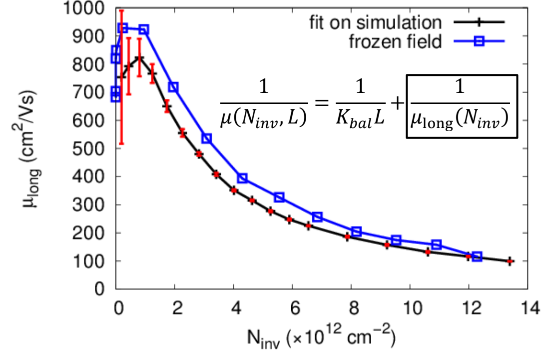

Figure 8. Black line: long channel mobility extracted from device simulations at different channel lengths, using the fitting formula shown in insert. In red: fitting standard error. Blue line with squares: mobility extracted from frozen field simulations.

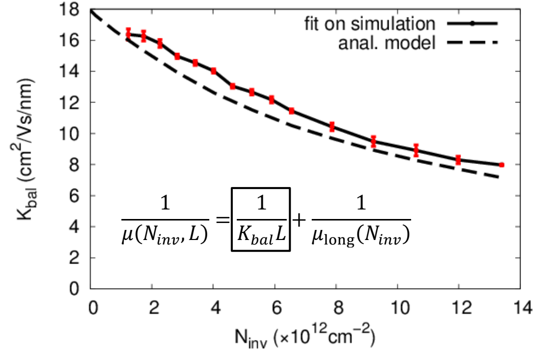

Figure 9. Ballistic mobility factor (Kbal) vs. inversion charge. Solid line: fit from Monte Carlo simulations. Dotted line: analytical model (Eq. 1).

respectively [4]. The extracted values of μ_{long} and K_{bal} are plotted as a function of N_{inv} in Figs. 8 and 9, respectively. Note that the "ballistic" component μ_{bal} not only results from the ballistic resistance, but also from the contact resistance, as discussed in the next section.

In addition, MSMC simulations with ballistic channel were performed: the comparison of the $I_d(V_g)$ characteristics with the diffusive case at $L = 100$ nm is shown in Fig. 3, and the effective mobility is shown in Fig. 6. These simulations provide an alternative method for evaluating μ_{bal}.

Fig. 8 also shows the mobility μ_{long} obtained from frozen field simulations, which is slightly larger than that extracted from the length dependence. This may be explained by the non-uniformity of the electric field in device simulations, and by a reduced effective channel length due to the junctions with source and drain.

IV. Comparison with Analytical Model

The MSMC "ballistic" effective mobility μ_{bal} was interpreted considering the sum of the ballistic and contact resistance:

$$\frac{1}{\mu_{\text{eff},bal}} = \frac{eN_{inv}W(R_{bal}+R_0)}{L} \quad (1)$$

In the effective mass approximation, the ballistic resistance is expressed by the following formula:

$$\frac{1}{WR_{bal}} = \sum_{v,n} \frac{e\sqrt{\pi m_y^v}(kT)^{\frac{3}{2}}}{\sqrt{2}\pi^2\hbar^2 V_{ds}} \left[\mathcal{F}_{1/2}\left(\frac{E_F - E_n^v}{kT}\right) - \mathcal{F}_{1/2}\left(\frac{E_F - eV_{ds} - E_n^v}{kT}\right)\right] \quad (2)$$

where W is the channel width. For each valley v, m_y^v is the transverse effective mass and E_n^v is the energy of subband n. $\mathcal{F}_{1/2}$ is the Fermi-Dirac integral of order ½. This formula is obtained by integrating over energy, for all the subbands, the ballistic current coming from both contacts. The formula is valid in all inversion regimes, in contrast to Shur's model [3]. In the linear regime (low source-drain bias V_{ds}), we recover the formula of Ref. [12]. In the non-degenerate regime and if all occupied valleys have the same effective mass, the product $N_{inv} \times R_{bal}$ is constant and given by Shur's formula. Here this product decreases at high inversion, as shown in Fig 9. In all cases, R_{bal} essentially varies as $1/N_{inv}$. It is dominant at low inversion and remains significant at high inversion, as discussed below.

Eq. 2 was evaluated using the subband energies E_n^v provided by the MSMC calculation. The effective mobilities obtained from MSMC simulations with ballistic channel were then fitted using Eq. 1. The best fit was obtained with a contact resistance $R_0 W = 35\ \Omega.\mu$m, assumed independent of the inversion charge. The agreement is good for all channel lengths, as shown in Fig. 6. The contact resistance is essentially due to surface roughness and impurity scattering in the access regions. At high inversion, the ballistic resistance R_{bal} is comparable to R_0.

Adding a term μ_{long} corresponding to the long channel mobility, the effective mobility for diffusive channel is given by:

$$\frac{1}{\mu_{\text{eff}}} = \frac{eN_{inv}W(R_0 + R_{bal})}{L} + \frac{1}{\mu_{\text{long}}(N_{inv})} \quad (3)$$

Keeping the same value for the contact resistance, $R_0W = 35\,\Omega.\mu\text{m}$, and using the diffusive mobility $\mu_{\text{long}}(N_{inv})$ previously extracted from MSMC simulations (see Fig. 8), Eq. 3 nicely reproduces the MSMC simulations with scattering in the channel, as shown in Fig. 5.

V. CONCLUSION

In conclusion, MSMC simulations of short channel devices show an apparent mobility degradation comparable to that observed in experiments, without additional scattering mechanism. The results at all channel lengths are well reproduced by an analytical model which combines the contact resistance, an accurate formula for the ballistic resistance, and the long channel mobility. Such a precise accounting for the ballistic resistance should improve the analytical and compact models used in circuit simulations, strengthening their physical basis for short channel devices. A basic Poisson/Schrödinger solver is sufficient to evaluate Eq. 2 and to calibrate the model for each device architecture. Such model could be further improved by including the gate voltage dependence of the access resistance, which is present in real devices.

ACKNOWLEDGMENT

This work was partially supported by the French National Research Agency (ANR) Quasanova and Noodles projects.

REFERENCES

[1] O. Weber et al., “Work-function Engineering in Gate First Technology for Multi-VT Dual-Gate FDSOI CMOS on UTBOX,” IEEE Int. Elec. Dev. Meet., pp. 3.4.1-3.4.4, Dec. 2010.

[2] A. Cros et al., “Unexpected mobility degradation for very short devices: A new challenge for CMOS scaling,” Int. Elec. Dev. Meet., pp. 663-666, Dec. 2006.

[3] M. S. Shur, “Low ballistic mobility in submicron HEMTs,” IEEE Elec. Dev. Lett., vol. 23, no. 9, pp. 511-513, Sept. 2002.

[4] K. Huet, J. Saint-Martin, A. Bournel, S. Galdin-Retailleau and P. Dollfus, “Monte Carlo Study of Apparent Mobility Reduction in Nano-MOSFETs,” European Solid State Device Research Conference, no. 37, pp. 382-385, Sept. 2007.

[5] K. Huet, J. Saint-Martin, A. Bournel, D. Querlioz and P. Dollfus, “Effect of access resistance on apparent mobility reduction in nano-MOSFET,” Int. conf. on Ult. Int. of Sil., no. 10, pp. 35-38, March 2009.

[6] G. Ghibaudo et al., “Electrical transport characterization of nano CMOS devices with ultra-thin silicon film,” Int. Work. on Junc. Tech., pp. 58-63, June 2009.

[7] F. Carosella, J. Saint-Martin, A. Bournel, S. Galdin-Retailleau and P. Dollfus, “Monte Carlo study of 2D electron gas transport including Pauli exclusion principle in highly doped silicon,” phys. stat. sol., vol. 5, pp. 98-101, Jan. 2008.

[8] J. Saint-Martin, A. Bournel, F. Monsef, C. Chassat and P. Dollfus, “Multi sub-band Monte Carlo simulation of an ultra-thin double gate MOSFET with 2D electron gas,” Semicond. Sci. and Tech., vol. 21, no. 4, p. L29, 2006.

[9] K. Romanjek, F. Andrieu, T. Ernst and G. Ghibaudo, “Improved split C-V method for effective mobility extraction in sub-0.1-µm Si MOSFETs,” IEEE Elec. Dev. Lett., vol. 25, no. 8, pp. 583-585, Aug. 2004.

[10] M. F. Hamer, “First-order parameter extraction on enhancement silicon MOS transistors,” IEE Proceedings I Solid-State and Elec. Dev., vol. 133, no. 2, pp. 49-54, April 1986.

[11] G. Ghibaudo, “New method for the extraction of MOSFET parameters,” Elec. Lett., vol. 24, no. 9, pp. 543-545, April 1988.

[12] M. Zilli, D. Esseni, P. Palestri and L. Selmi, “On the Apparent Mobility in Nanometric n-MOSFETs,” IEEE Elec. Dev. Lett., vol. 28, no. 11, pp. 1036-1039, Nov. 2007.